Relaxation of Segment Orientation in Dilute Polymer Solution. Interpretation of ^{13}C T_1 and NOE Experiments on Dilute Poly[(*R*,*S*)-3,7-dimethyl-1-octene] and Poly[(*R*,*S*)-3-methyl-1-octene]

Angelo Perico

Centro Studi Chimico-Fisici di Macromolecole Sintetiche e Naturali del CNR e Istituto di Chimica Industriale dell'Università di Genova, Corso Europa 30, 16132 Genova, Italy

Angelina Altomare, Donata Catalano, Mauro Colombani, and Carlo Alberto Veracini*

Dipartimento di Chimica e Chimica Industriale dell'Università di Pisa, Via Risorgimento 35, 56100 Pisa, Italy

Received February 21, 1990

ABSTRACT: The ^{13}C spin–lattice relaxation time, T_1, and the nuclear Overhauser effect, NOE, of CH_n groups in poly[(*R*,*S*)-3,7-dimethyl-1-octene] and in poly[(*R*,*S*)-3-methyl-1-octene] have used in order to probe via the calculated spectral densities various theoretical models for the segmental relaxation of polymers in dilute solutions. The experimental data relative to the lateral chains have been treated in the framework of the Lipari–Szabo theory. Following the optimum Rouse–Zimm local dynamics (ORZLD) model, high values of the orientation persistence length, p, for the backbone chain have been determined for both polymers (p = 39 and 42 monomeric units, respectively), while the order continuously and substantially decreases along the lateral chains.

I. Introduction

The spin relaxation times of the nuclei on a polymer chain in solution are sensitive to the chain segmental dynamics in the nanosecond time domain. Spin–lattice and spin–spin relaxation times, T_1 and T_2, and the nuclear Overhauser effect, NOE, of ^{13}C in CH_n groups over a range of resonance frequencies are the important NMR measurements to probe this segmental dynamics.[1] The information is contained in the spectral density, which is the Fourier transform of the second-order orientational time correlation function of the relaxing dipoles. The crucial point for a quantitative interpretation of the NMR relaxation experiments is the availability of a confident dependence of the time correlation function on the conformational details of the chain. In the nanosecond time domain, the proper dynamic approach to the time correlation function is based on the diffusion equation in the polymer configuration space, or on the Kramers rate equation in the diffusion limit.[2,3]

Here we will take advantage of some advances in the diffusion theory of segment relaxation[2] in order to give a structural interpretation of T_1 and NOE experiments on poly[(*R*,*S*)-3,7-dimethyl-1-octene] (DMO)[4-6] and poly[(*R*,*S*)-3-methyl-1-octene] (MO) in terms of the stiffness of the backbone and of the side-chain correlation.

II. Dynamic Models for the Spectral Density

The dominant relaxation mechanism for ^{13}C in CH_n groups is the dipolar one. The longitudinal and transverse relaxation times and NOE due to this mechanism are given as functions of the spectral density by the following expressions:[7]

$$T_1(j)^{-1} = (n/20)\hbar^2\gamma_C^2\gamma_H^2 r^{-6}[J_j(\omega_C - \omega_H) + 3J_j(\omega_C) + 6J_j(\omega_C + \omega_H)] \quad (1)$$

$$T_2(j)^{-1} = (n/40)\hbar^2\gamma_C^2\gamma_H^2 r^{-6}[4J_j(0) + J_j(\omega_C - \omega_H) + 3J_j(\omega_C) + 6J_j(\omega_H) + 6J_j(\omega_C + \omega_H)] \quad (2)$$

$$\mathrm{NOE}_j = 1 + (\gamma_H/\gamma_C)[6J_j(\omega_C + \omega_H) - J_j(\omega_C - \omega_H)]/[J_j(\omega_C - \omega_H) + 3J_j(\omega_C) + 6J_j(\omega_C + \omega_H)] \quad (3)$$

where γ_C and γ_H are the magnetogyric ratios of the ^{13}C and ^1H nuclei, respectively, ω_C and ω_H are their resonance frequencies, and r is the C–H distance. The label j identifies the ^{13}C nucleus, and n is the number of protons directly bound to it. Following our numbering of atoms (see Figure 1), j = 1 corresponds to the backbone carbon of any monomeric unit attached to the side chain. The spectral density, obtained as an average from all the ^{13}C nuclei in position j along the polymer chain, is given by the Fourier transform

$$J_j(\omega) = 2\,\mathrm{Re}\int_0^\infty G_j(t)\exp(i\omega t)\,dt \quad (4)$$

of the time correlation function $G_j(t)$ relative to the dipolar relaxation of the ^{13}C in position j. The relaxing dipoles of the backbone polymer chain are assumed to be rigidly attached to the effective bond, spanning a monomer (the segment vector of the polymer model), and therefore we can approximate the relaxation of these dipoles with the relaxation of the relative segment vector $\mathbf{l}_i$, in position i along the chain. This relaxation is described by the second-order orientation time correlation function $P_2^i(t)$:

$$P_2^i(t) = (3/2)\langle\cos^2\theta_i(t)\rangle - 1/2 \quad (5)$$

with $\theta_i(t)$ the angle that the relaxing segment $\mathbf{l}_i$ spans in a time t.

In the case of a ^{13}C in position j on a lateral chain and with the assumption of independence of the backbone and side-chain motions, the suitable correlation function has the form

$$G_{ij}(t) = P_2^i(t)g_j(t) \quad (6)$$

The term $g_j(t)$ comes from restricted motion relative to a reference frame fixed on the backbone chain and may be written, according to Lipari and Szabo,[8] as

$$g_j(t) = S_j^2 + (1 - S_j^2)\exp(-t/\tau_j) \quad (7)$$

0024-9297/90/2223-4912$02.50/0

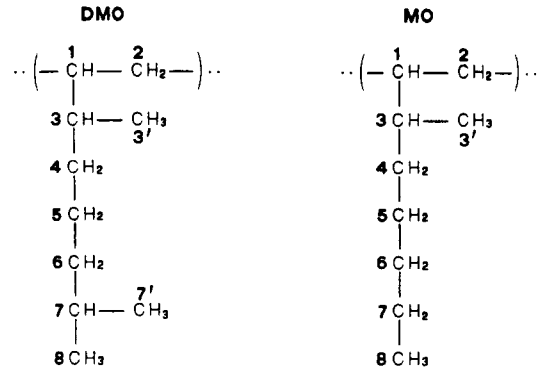

Figure 1. Structures of poly[(*R*,*S*)-3,7-dimethyl-1-octene] (DMO) and poly[(*R*,*S*)-3-methyl-1-octene] (MO) and numbering of atoms.

with S_j the generalized order parameter of the side group in position j. For $S_j^2 = 1$ the side group is rigidly attached to the backbone, and the relaxation is described only by the relaxation of the backbone bond vector $\mathbf{l}_i$, while for $S_j^2 = 0$ the side-chain motion is completely unrestricted and approximated by a time correlation function of correlation time τ_j.

Note that in this rough approximation the different carbon nuclei of the backbone on the same monomeric unit ($j = 1$ and $j = 2$ according to the numbering adopted here) have the same time correlation function, equal to that of the effective bond vector. In a more accurate model, not tried here, the $j = 2$ ^{13}C is allowed to undergo restricted motion relative to the effective bond vector, with an order parameter S_2^2 and a correlation time τ_2 according to eq 7.

In general, what is measured is an average of $G_{ij}(t)$ over all the equivalent ^{13}C in the chain:

$$G_j(t) = (n-1)^{-1}\sum_{i=1} G_{ij}(t) - G_{n/2,j}(t) \cong P_2^{n/2}(t) g_j(t) \qquad (8)$$

where the sum is over all the monomers in the chain and the relationship on the right-hand side of eq 8 is obtained for large n.

By fitting the experimental results for T_1 and NOE at different frequencies with eq 8, combined with eqs 4, 1, and 3, the structural parameters describing $P_2^{n/2}(t)$ and the quantities S_j^2 and τ_j relative to the side chains can be determined.

III. Models for $P_2^{n/2}(t)$

Theoretical models of the second-order time correlation function for rigid bodies based on the diffusion equation were solved in the early thirties,[9,10] but they are unrealistic for actual flexible polymers. For a sphere or a rod the segment relaxation is described by a simple exponential decay

$$P_2(t) = \exp(-3t/\tau) \qquad (9)$$

with τ the characteristic rotational time for the rod or sphere.

For flexible polymers the popular VJGM model,[11] based on the assumption of a chain performing three-bond motions on a tetrahedral lattice, is characterized by a simple universal function with two characteristic times, τ_1 and τ_2, relative to the three-bond jump motion and to the out-of-lattice motions, respectively:[11]

$$P_2(t) = \exp(-t/\tau_2)\exp(t/\tau_1)\,\mathrm{erfc}\,[(t/\tau_1)^{1/2}] \qquad (10)$$

with erfc (x) the complementary error function. As for all the lattice models, the first- and second-order time correlation functions are identical. In addition, this model gives an unrealistic infinite first derivative at $t = 0$. For these reasons this model cannot be accepted.[12]

Table I
$P_2^{n/2}(t)$ for a Gaussian Chain in Partial Draining Conditions[a] as a Function of τ[b]

τ	$P_2^{n/2}(t)$	τ	$P_2^{n/2}(t)$	τ	$P_2^{n/2}(t)$
0.01	0.9388198	0.70	0.1392283	6.00	0.0057207
0.05	0.7727808	0.80	0.1161253	7.00	0.0046292
0.10	0.6336247	0.90	0.0981468	8.00	0.0038572
0.20	0.4540498	1.00	0.0839555	9.00	0.0032857
0.30	0.3411229	2.00	0.0282250	10.0	0.0028477
0.40	0.2642675	3.00	0.0152474	15.0	0.0016458
0.50	0.2095585	4.00	0.0100714	20.0	0.0011165
0.60	0.1694004	5.00	0.0073633		

[a] $\zeta_r = 0.25$. [b] $\tau = \sigma t$.

The Hall–Helfand model,[13] based on a Kramers approach in the diffusion limit, gives a solution in terms of a universal two-parameter function for the nonobservable conformational time correlation function, $C(t)$. This is in turn assumed to approximate the measurable $P_2(t)$:

$$P_2(t) \cong C(t) = \exp(-t/\tau_2)\exp(-t/\tau_1) I_0(t/\tau_1) \qquad (11)$$

with τ_1 and τ_2 related to correlated and isolated conformational jumps, respectively, and $I_0(t/\tau_1)$ the modified Bessel function of zero order. This function does not have the unrealistic short-time behavior of the VJGM function and has been used for the interpretation of fluorescence anisotropy decay[12] and NMR relaxation experiments,[14,15] with τ_1 and τ_2 as parameters to describe polymer and solvent effects.[14,15]

Only recently the measurable orientational time correlation functions for flexible and semiflexible polymers could be calculated exactly by using the optimum Rouse–Zimm approximation (ORZ) to the generalized diffusion equation in the full polymer configurational space.[2,16] As we use these results to interpret the T_1 and NOE experiments on DMO and MO, we summarize and discuss this approach, to which we will refer in the following as the ORZ local dynamics (ORZLD).

The chain model adopted has $n - 1$ effective bonds

$$\mathbf{l}_i = \mathbf{R}_i - \mathbf{R}_{i-1} \qquad i = 1, ..., n-1 \qquad (12)$$

of root mean square length l and n beads of friction coefficient ζ and intramolecular potential of mean force $V(\{\mathbf{R}_i\})$, with $\mathbf{R}_i$ the laboratory coordinates of bead i. Θ conditions are assumed for simplicity. The time correlation function $P_2(t)$ is obtained as a universal function of the segment vector time correlation function $M_1^i(t)$:

$$P_2^i(t) = 1 - 3\{x^2 - x^3(\pi/2)[1 - (2/\pi)\arctan x]\} \qquad (13)$$

$$x = [1 - (M_1^i(t))^2]^{1/2}/M_1^i(t)$$

where $M_1^i(t)$ is

$$M_1^i(t) = \langle \mathbf{l}_i(t)\cdot\mathbf{l}_i(0)\rangle/l^2 = \sum_{a=1}(Q_{i,a} - Q_{i-1,a})^2 \mu_a^{-1} \exp(-\sigma\lambda_a t) \qquad (14)$$

The constant

$$\sigma = 3k_B T/l^3\zeta \cong 2k_B T/\pi\eta_0 l^3 \qquad (15)$$

with η_0 the solvent viscosity, is the characteristic bond rate constant of the model, expected to be an upper limit to the jump transition rate. The quantities λ_a and $\mathbf{Q}$ are the eigenvalues and the eigenvector matrix, respectively, of the product $\mathbf{H}\cdot\mathbf{A}$ of the matrix of the hydrodynamic interaction $\mathbf{H}$ and the structural matrix $\mathbf{A}$. The quantities μ_a are the diagonal elements of the diagonal matrix $\mathbf{Q}^T\cdot\mathbf{A}\cdot\mathbf{Q}$.

The **H** and **A** matrices are defined as follows:

$$H_{ij} = \delta_{ij} + \zeta_r\langle 1/R_{ij}\rangle(1-\delta_{ij}) \tag{16}$$

with

$$\zeta_r = \zeta/6\pi\eta_0 l \tag{17}$$

the hydrodynamic interaction strength ($\zeta_r = 0.25$ for a dilute Θ solution) and

$$\mathbf{A} = \mathbf{M}^T\begin{pmatrix} 0 & 0 \\ 0 & \mathbf{U} \end{pmatrix}\mathbf{M} \tag{18}$$

where

$$\mathbf{M} = \begin{pmatrix} 1/n & 1/n & 1/n & . & \dots \\ -1 & 1 & 0 & . & \dots \\ 0 & -1 & 1 & 0 & \dots \\ . & . & . & . & \dots \end{pmatrix} \tag{19}$$

The matrix **U** is the inverse of the static bond correlation matrix

$$\mathbf{U}^{-1} = \langle \mathbf{l}_i \cdot \mathbf{l}_j\rangle/l^2 \tag{20}$$

The equilibrium averages $\langle 1/R_{ij}\rangle$ and $\langle \mathbf{l}_i \cdot \mathbf{l}_j\rangle/l^2$ are calculated by the intramolecular potential $V(\{\mathbf{R}_i\})$

$$\langle \mathbf{l}_i \cdot \mathbf{l}_j\rangle/l^2 = N\int \mathrm{d}\{\mathbf{R}_i\} \exp[-V(\{\mathbf{R}_i\})/k_BT]\langle \mathbf{l}_i \cdot \mathbf{l}_j\rangle/l^2 \tag{21}$$

$$\langle 1/R_{ij}\rangle = N\int \mathrm{d}\{\mathbf{R}_i\} \exp[-V(\{\mathbf{R}_i\})/k_BT](1/R_{ij}) \tag{22}$$

and

$$N^{-1} = \int \mathrm{d}\{\mathbf{R}_i\} \exp[-V(\{\mathbf{R}_i\})/k_BT] \tag{23}$$

Note that in the straightforward case of a Gaussian chain

$$\langle \mathbf{l}_i \cdot \mathbf{l}_j\rangle/l^2 = \delta_{ij} \tag{24}$$

and in the free-draining limit

$$H_{ij} = \delta_{ij} \tag{25}$$

In these hypotheses eq 14 is easily summed[17] to give for the central segment

$$M_1^{n/2}(t) = \exp(-2\sigma t)I_0(2\sigma t) \tag{26}$$

which is the relevant part of the Hall–Helfand function (see eq 11), with τ_1 identified as $(2\sigma)^{-1}$. This result shows that the Hall–Helfand function takes into account simply the connectivity of an infinte Gaussian chain in the free-draining limit for $M_1(t)$. However, even in this limit, different expressions are required for different time correlation functions (compare eq 13 with eq 14). In addition, as draining strongly affects the eigenvalues λ_a, a relevant draining effect on $P_2(t)$ is expected. Numerical results for $P_2^{n/2}(t)$ for a Gaussian chain in partial draining conditions ($\zeta_r = 0.25$) are reported in Table I as a function of the adimensional variable τ:

$$\tau = \sigma t \tag{27}$$

This table is independent of n for $n > 50$ and gives a correlation time

$$T = \int_0^\infty P_2(t)\,\mathrm{d}t = 0.452\sigma^{-1} \tag{28}$$

A fitting of the experimental values of T_1 and NOE (see eqs 1 and 3) allows one to find the parameter σ and, via eq 15, the segment length describing the stiffness of the chain.

In the case of a freely rotating chain model with an effective bond length l_0 and a valence angle θ

$$g = -\cos\theta \tag{29}$$

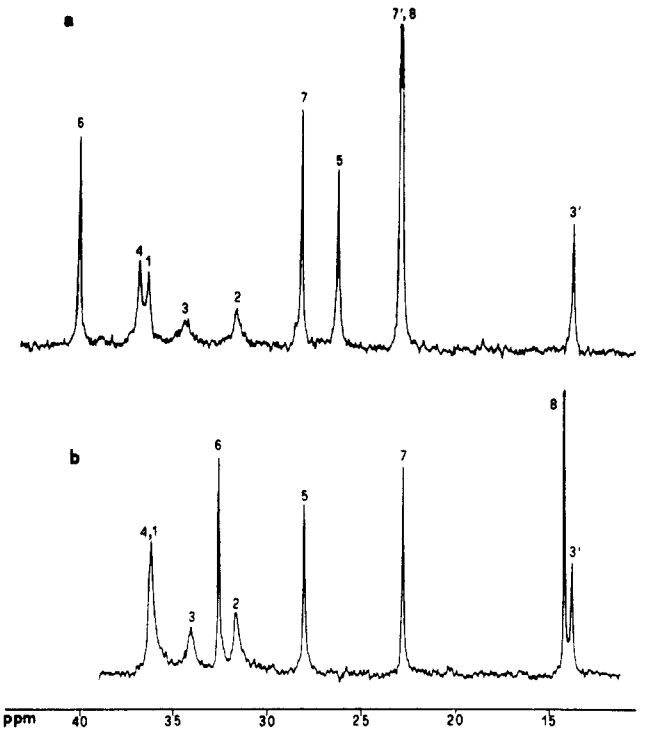

Figure 2. Proton-decoupled ^{13}C NMR spectra of (a) poly[(*R*,*S*)-3,7-dimethyl-1-octene] and (b) poly[(*R*,*S*)-3-methyl-1-octene] in $CDCl_3$ solution at 75.4 MHz and T = 40 °C.

is the stiffness parameter and

$$p = l_0(1-g)^{-1} \tag{30}$$

is the persistence length. The ORZ dynamics for a long freely rotating chain is equivalent to that of a Gaussian chain with a renormalized segment length

$$l = l_0(1+g)^{1/2}(1-g)^{-1/2} \tag{31}$$

Therefore, a fitting of the experimental data based on a freely rotating chain model for the polymer backbone gives directly the number of effective bonds spanned by a persistence length.

For vinyl polymers, l_0 may be chosen as the modulus of the vector sum of the two bonds spanning the monomeric unit (l_0 = 2.515 Å for DMO and MO). The use of rotational isomeric state (RIS) polymer models in the ORZLD[18] could enable one to include more local details and to differentiate the backbone motion of ^{13}C j = 1 and ^{13}C j = 2.

IV. Experimental Section

Carefully degassed solutions of DMO and MO in $CDCl_3$ (5% by weight) were investigated at 30, 35, 40, and 45 °C. ^{13}C spectra were recorded at 25.2 (only in the case of DMO), 50.3, and 75.4 MHz, using Varian XL100, Gemini 200, and VXR 300 spectrometers, respectively, with complete proton decoupling. The spectra of DMO and MO obtained at 40 °C and 75.4 MHz are shown in Figure 2.

T_1, the longitudinal relaxation time, was determined for all the peaks for which this was possible at the three frequencies in the case of DMO and at 50.3 and 75.4 MHz in the case of MO, using the standard inversion–recovery technique. A composite pulse was adopted for magnetization inversion, together with an accurately calibrated 90° pulse.

NOE, the ^{13}C nuclear Overhauser enhancement, was determined for all the peaks for which this was possible at 50.3 and 75.4 MHz for both compounds, using the standard gated decoupling technique.

The data were processed by the standard instrumental software.

The carbon peak assignment of DMO is reported in the literature[6] for the polymer in solution and in the solid state (the

Table II
Experimental Values of T_1 and NOE of ^{13}C in Poly[(*R,S*)-3,7-dimethyl-1-octene]

carbon	chem shift, ppm	25.2 MHz	50.3 MHz		75.4 MHz	
		nT_1,[b] s	nT_1,[b] s	NOE[c]	nT_1,[b] s	NOE[c]
1	35.88		0.140	2.020	0.173	1.750
2	31.22			1.954	0.174	
3	33.93				0.173	
3′	13.68		1.520	1.961	1.860	2.158
4	36.33		0.390	2.080	0.516	2.054
5	25.98	0.566	0.716	2.157	0.692	2.082
6	39.57	0.728	1.270	2.400	1.294	2.361
7	27.88	1.709	1.794	2.346	1.383	2.092
7′, 8	22.66, 22.76	3.666	4.485	2.755	4.920	2.567

[a] Uncertainties on experimental chemical shifts are ca. 0.02 ppm. [b] The quantity experimentally determined is T_1. n is the number of protons bound to the carbon nucleus. The experimental uncertainties on T_1 values range from 0.01 to 0.07 s. [c] The experimental uncertainties on NOE values are ca. 0.08.

Table III
Experimental Values of T_1 and NOE of ^{13}C in Poly[(*R,S*)-3-methyl-1-octene]

carbon	chem shift,[a] ppm	50.3 MHz		75.4 MHz	
		nT_1,[b] s	NOE[c]	nT_1,[b] s	NOE[c]
1	35.50			0.276	1.692
2	31.46	0.156	1.883	0.216	1.733
3	33.90	0.188	1.532	0.241	1.716
3′	13.73	1.448	2.281	1.971	2.213
4	35.95	0.433	2.317	0.536	2.049
5	27.88	0.880	2.519	1.101	2.323
6	32.34	1.517	2.393	1.819	2.339
7	22.64	3.382	2.351	3.630	2.303
8	14.10	7.302	2.520	8.159	2.552

[a-c] Same footnotes as in Table II.

spectra are quite similar) based on chemical shift additivity rules[19] suitably modified in order to account for conformational effects.[20,21] The assignment was also checked with the help of the DEPT technique,[6] a test experiment for the number of protons attached to each carbon.[22] In the case of MO, the carbon peaks were assigned by using the same additivity rules. The experimental values of the chemical shifts at 40 °C and the peak assignments are reported in Tables II and III for the two polymers, respectively.

Only the T_1 and NOE data obtained at 40 °C, also reported in Tables II and III, were used for the test of dynamic models discussed in the following section.

Unfortunately, there are some blanks in the tables. In fact, the peaks relative to carbons 2 and 3 of DMO are rather weak and broad; therefore, it was sometimes impossible to extract well-determined values of T_1 and NOE for these nuclei. The weak peak relative to carbon 1 of MO is partially hidden by the much more intense one assigned to carbon 4.

V. Results and Discussion

The relaxation data of Tables II and III have been used in order to test the correlation functions discussed in the theoretical section. In particular, the following models were adopted for describing the backbone relaxation.

(1) Simple exponential decay $P_2(t) = \exp(-t/\tau_M)$: In this case τ_M, the correlation time relative to the backbone motion, is the parameter to be determined by the fitting of the relaxation data.

(2) The Hall–Helfand model for conformational dynamics (see eq 11): Here the fitting parameters are τ_1 and τ_2 (or, as usually done, τ_1 and the ratio τ_2/τ_1).

(3) The ORZLD model for a simple Gaussian chain in partial draining conditions (see eq 13): In this case the fitting parameter is σ.

The experimental data relative to carbons 1 and 2 were so analyzed on the basis of eqs 1 and 3 combined with eq 4 and with three different expressions of the second-order time correlation function.

The Lipari–Szabo model (see eq 7) was adopted in conjunction with these three expressions, as given in eqs 6 and 8, in order to describe the relaxation of the side-chain carbon nuclei. Thus the parameter(s) characterizing the $P_2^i(t)$ function were fixed as found from the experimental data relative to carbons 1 and 2, and S_j^2 and τ_j were determined for each carbon nucleus of the lateral chain by reproducing the T_1 and NOE data via eqs 1 and 3, respectively, combined with eqs 4 and 8.

In all cases a standard least-squares fitting procedure was applied, with four or five data used to determine one or two unknown parameters.

The interpretation of T_1 data on the basis of eq 3 requires one to fix or determine the C–H bond distance. We verified that, as far as the backbone carbon nuclei are concerned, the quality of the fittings obtained changes by changing such distance within a reasonable range of values, but the resulting values of the best-fit parameters do not vary significantly. As far as the lateral chain is concerned, the variation of the C–H distance can be always compensated by a changing of the S_j^2 and τ_j parameters. We have fixed the C–H distance to 1.09 Å throughout the present work.

It may be noted that in the few cases where a comparison is possible, the experimental datum relative to carbon 1 coincides, within the limits of the experimental error, with the corresponding datum relative to carbon 2. This agrees with the theoretical assumption of rigidity for the monomeric unit in the backbone chain. The data from carbon 1 or 2 are therefore used indifferently in the analysis. Moreover, the experimental data relative to carbon 3 are very similar to those of carbons 1 and 2, this indicating the substantial stiffness of the fragment C_3–C_1–C_2.

Independently of the model applied, a satisfactory reproduction of the experimental data is always obtained; that is, in most cases, the differences between the experimental and computed values do not exceed the experimental error. Moreover, reasonable best-fit parameters are found in every case; therefore, no discrimination between the three models for the backbone relaxation can be performed on the basis of the fitting results.

In Table IV the best-fit parameters concerning the backbone motion of DMO and MO are reported for the three models considered. The parameters τ_M and σ of models 1 and 3, respectively, can be interpreted either in terms of the stiffness parameter g or in terms of the persistence length p, according to eqs 28 and 15 and eqs 30 and 31 (see Table IV). Within this procedure, method 1 simply fits the correlation time of the ORZLD model, while method 3 fits the whole correlation function. Since

Table IV
Best-Fit Parameters for the Two Polymers and the Three Theoretical Models Considered (Results for the Backbone Polymer Chains)

polymer	model[a]	τ_M,[b] s	σ, s^{-1}	τ_1, s	τ_2/τ_1	l,[c] Å	g[d]	p/l_0[e]
DMO	1	$8.94\ (36) \times 10^{-10}$	5.05×10^8			22.2	0.975	39
	2			$6.43\ (2) \times 10^{-10}$	63 (2)			
	3		$5.05\ (3) \times 10^8$			22.2	0.975	39
MO	1	$9.91\ (82) \times 10^{-10}$	4.56×10^8			22.9	0.976	42
	2			$6.97\ (2) \times 10^{-10}$	58 (4)			
	3		$4.48\ (2) \times 10^8$			23.1	0.977	43

[a] According to the numbering in the text, section V: (1) simple exponential decay; (2) Hall–Helfand model for conformational dynamics; (3) the ORLZD model for a simple Gaussian chain in partial draining conditions. [b] Following eq 28, $\tau_M = 0.452\sigma^{-1}$. [c] Following eq 15, $l^3 = 2k_BT/\pi\eta_0\sigma \simeq 5.505 \times 10^{12}/\sigma$ if $T = 40$ °C and $\eta_0 = 5 \times 10^{-3}$ P. [d] g is determined through eq 31, $(l/l_0)^2 = (1+g)/(1-g)$; the effective bond length l_0 is 2.515 Å if a C–C bond distance of 1.54 Å and a C–C–C angle of 109.47° are assumed. [e] Following eq 30, $p/l_0 = (1-g)^{-1}$; p/l_0 is the number of effective bonds for which there is "persistence" of the orientation.

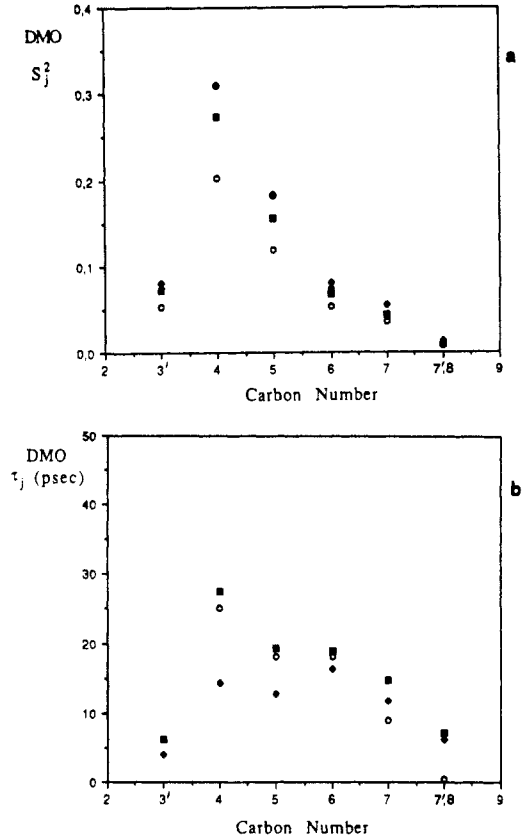

Figure 3. Generalized order parameter S_j^2 (a) and correlation time τ_j (b) as functions of the carbon number j for the lateral chain of poly[(*R*,*S*)-3,7-dimethyl-1-octene]. The Lipari–Szabo model (eq 7) is used in conjunction with models 1 (○), (2) (■), and (3) (◆). The standard deviations on S_j^2 range from 1/10 to 1/5 of the value computed for this parameter; standard deviations on τ_j are about 1/4 of the value computed for τ_j.

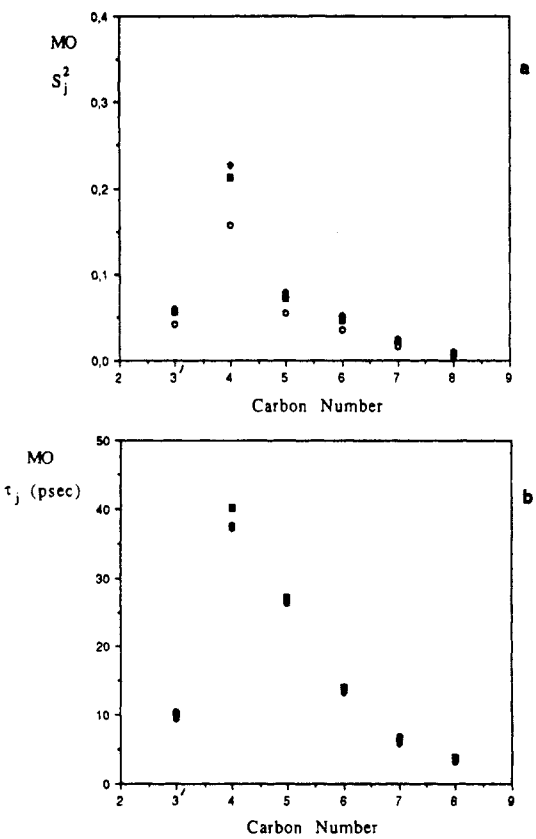

Figure 4. Same as Figure 3 for the lateral chain of poly[(*R*,*S*)-3-methyl-1-octene].

no appreciable difference emerges between the results of models 1 and 3, we can conclude that the available experimental data are sensitive to the correlation time of the ORZLD model (see eq 27) rather than to the details of the correlation function. As far as the results of the Hall–Helfand model are concerned, they seem acceptable when compared with the values of τ_1 and τ_2/τ_1 reported by Viovy et al. for polystyrene.[23] However, the connection between these values and the degree of stiffness (or flexibility) of the polymer is not direct. Following the discussion of eq 26 in section II, the Hall–Helfand approximation amounts to taking $P_2^i \cong M_1^i$, while when τ_2/τ_1 is large, τ_1 may be identified with $0.5\sigma^{-1}$. Note that in this case τ_1 is not very different from the correlation time for $P_2^i(t)$, which is $0.452\sigma^{-1}$ (see eq 28). However, the correlation time for the Hall–Helfand model function increases with increasing τ_2/τ_1 and becomes much larger than τ_1 for high values of τ_2/τ_1. The origin of τ_2 remains to be clarified on a molecular basis.

We now examine the indications yielded by models 1 and 3 in terms of persistence length. The two polymers show similar stiffness, but a slightly higher value of p is exhibited by MO. This could be ascribed to structural reasons: the greater bulkiness of the lateral chain in the case of DMO might result in a steric perturbation of the backbone conformational order. The difference is small, however, and could be simply due to a slightly different stereoregularity of the two polymers. It must also be observed that the persistence length obtained from these data is probably overestimated: a change in the friction coefficient by a factor of 2, not unreasonable in this case because of the bulkiness of the lateral chain, could reduce the persistence length from 40 to 32 effective bonds.

The results relative to the lateral chain carbon nuclei, obtained according to the Lipari–Szabo treatment, are summarized in Figures 3 and 4 for DMO and MO, respectively. For both polymers the generalized order parameter S_j^2 decreases as a function of the carbon number

j along the side chain, with an exponential-like trend. (The value of S_3^2 is computed to be >0.9.) This is the behavior that one expects to find for an isolated chain rigidly anchored at only one extremity.[24] The same trend is exhibited by the effective correlation time τ_j in MO, while in DMO the trend of τ_j seems to reflect some steric hindrance to internal rotation, possibly due to the side-chain terminal ramification. The notable exception to all these trends is shown by the methyl carbon nucleus with $j = 3'$ (very low order parameter and correlation time) and is not unexpected, since particularly free internal rotation is allowed for the methyl group.

The overall picture emerging from the present study permits us to describe the two macromolecules considered here as highly ordered, with a substantial persistence of the orientation of the effective bonds even in solution, while the orientational order continuously and noticeably decreases along the side chains. This picture was also suggested by the close resemblance, discussed in ref 6, between the ^{13}C spectrum of DMO in solution and its high-resolution spectrum in the solid state. Moreover, our conclusion is in good agreement with previous studies concerning the polymerization stereochemistry of *rac*-3,7-dimethyl-1-octene[5] and the conformation in solution of the polymers of optically active DMO, investigated by chirooptical methods.[4] According to ref 5, in fact, macromolecules deriving from racemic monomers not only are isotactic but also show a high regularity in the side chains, due to the stereoselective polymerization. In ref 4 it is shown that the main chain is highly helical and ordered, while lateral chains have a relatively high flexibility.

Acknowledgment. We are grateful to Professors F. Ciardelli and C. Carlini for useful suggestions and to MPI (Rome) for financial support.

References and Notes

(1) Heatley, F. In *Annual Reports on NMR Spectroscopy*; Academic Press: London, 1986; Vol. 17, p 179.
(2) Perico, A. *Acc. Chem. Res.* **1989**, *22*, 336.
(3) Helfand, E. In *Photophysical and Photochemical Tools in Polymer Science*; Winnik, M. A., Ed.; Nato ASI Series C182, Dordrecht, 1986; p 152.
(4) Pino, P.; Ciardelli, F.; Lorenzi, G. P.; Montagnoli, G. *Makromol. Chem.* **1963**, *61*, 207.
(5) Pino, P.; Ciardelli, F.; Montagnoli, G. *J. Polym. Sci., Part C* **1968**, *16*, 3265.
(6) Sacchi, M. S.; Tritto, I.; Locatelli, P.; Zetta, L.; Ferro, D.; Forster, H. *Macromolecules* **1986**, *19*, 1634.
(7) Wittebort, R. J.; Szabo, A. *J. Chem. Phys.* **1978**, *69*, 1722.
(8) Lipari, G.; Szabo, A. *J. Am. Chem. Soc.* **1982**, *104*, 4546.
(9) Debye, P. *Polar Molecules*; Dover: New York, 1929.
(10) Perrin, f. *J. Phys. Radium* **1934**, *V*, 497; **1936**, *VII*, 1.
(11) Valeur, B.; Jarry, J. P.; Geny, F.; Monnerie, L. *J. Polym. Sci., Polym. Phys. Ed.* **1975**, *13*, 667, 675.
(12) Monnerie, L.; Viovy, J. L. In *Photophysical and Photochemical Tools in Polymer Science*; Winnik, M. A., Ed.; Nato ASI Series C182, Dordrecht, 1986; p 193.
(13) Hall, C. K.; Helfand, E. *J. Chem. Phys.* **1982**, *77*, 3275.
(14) Hung, C.-C.; Shibata, J. W.; Tarpey, M. F.; Jones, A. A.; Porco, J. A.; Inglefield, P. T. *Anal. Chim. Acta* **1986**, *189*, 167.
(15) Hung, C.-C.; Shibata, J. W.; Jones, A. A.; Inglefield, P. T. *Polymer* **1987**, *28*, 1062.
(16) Perico, A.; Guenza, M. *J. Chem. Phys.* **1985**, *83*, 3103; **1986**, *84*, 510.
(17) Perico, A. *J. Chem. Phys.* **1988**, *88*, 3996.
(18) Perico, A.; Ganazzoli, F.; Allegra, G. *J. Chem. Phys.* **1987**, *87*, 3677.
(19) Lindeman, L. P.; Adams, J. Q. *Anal. Chem.* **1971**, *43*, 1245.
(20) Ferro, R. D.; Ragazzi, M. *Macromolecules* **1984**, *17*, 485.
(21) Ferro, R. D.; Ragazzi, M.; Provasoli, A. Proceedings of the VII Convegno Italiano di Scienza delle Macromolecole, Galzignano, Italy, 1985, p 141.
(22) Doddrell, D. M.; Pegg, D. T.; Bendall, M. R. *J. Magn. Reson.* **1982**, *48*, 323.
(23) Viovy, J. L.; Monnerie, L.; Brochon, J. C. *Macromolecules* **1983**, *16*, 1845.
(24) Charvolin, J.; Tardieu, A. In *Solid State Physics*; Seitz, F., Turnbull, D., Eds.; Academic Press: New York, 1978; p 209 and refs 80 and 81 therein.